



SECURITY CLASSIFICATION OF THIS PAGE

REPORT DOCUMENTATION PAGE				
1a. REPORT SECURITY CLASSIFICATION <b>UNCLASSIFIED</b>		1b. RESTRICTIVE MARKINGS		
2a. SECURITY CLASSIFICATION AUTHORITY		3. DISTRIBUTION/AVAILABILITY OF REPORT Approved for public release; distribution unlimited.		
2b. DECLASSIFICATION/DOWNGRADING SCHEDULE				
4. PERFORMING ORGANIZATION REPORT NUMBER(S)  NRL Report 8793		5. MONITORING ORGANIZATION REPORT NUMBER(S)		
6a. NAME OF PERFORMING ORGANIZATION Naval Research Laboratory	6b. OFFICE SYMBOL (If applicable) Code 5120	7a. NAME OF MONITORING ORGANIZATION Naval Air Systems Command		
6c. ADDRESS (City, State and ZIP Code)  Washington, DC 20375		7b. ADDRESS (City, State and ZIP Code)  Washington, DC 20361		
8a. NAME OF FUNDING/SPONSORING ORGANIZATION Naval Air Systems Command	8b. OFFICE SYMBOL (If applicable)	9. PROCUREMENT INSTRUMENT IDENTIFICATION NUMBER		
8c. ADDRESS (City, State and ZIP Code)  Washington, DC 20361		10. SOURCE OF FUNDING NOS.		
		PROGRAM ELEMENT NO. 62749N	PROJECT NO. WF59-552000	TASK NO. WORK UNIT NO. 51-0351-04
11. TITLE (Include Security Classification) (See Page ii)				
12. PERSONAL AUTHOR(S) Michael J. Buckingham				
13a. TYPE OF REPORT Interim	13b. TIME COVERED FROM Dec. '82 TO Sept. '83	14. DATE OF REPORT (Yr., Mo., Day) 1984 March 19	15. PAGE COUNT 26	
16. SUPPLEMENTARY NOTATION (See Page ii)				
17. COSATI CODES		18. SUBJECT TERMS (Continue on reverse if necessary and identify by block number)		
FIELD	GROUP	SUB. GR.		
		Acoustic propagation; wedge		
19. ABSTRACT (Continue on reverse if necessary and identify by block number)				
<p>A new solution for the acoustic field produced by a point source in a wedge-shaped ocean channel with pressure-release boundaries is presented. The solution is in the form of a sum of normal modes, which reduces in the immediate vicinity of the source point to the free-field solution for a point source. The radiation field associated with each mode forms a well-defined beam which diverges as the energy propagates out towards deep water. Outside the beam, shadow zones are formed, where there is essentially no energy in the mode. The modal beams are nested together, with the inner and outer beams having the highest and lowest mode numbers, respectively. Thus, the spatial extent of the field in the direction parallel to the shore line is determined by the lowest order mode. The modal beams are interpreted in terms of rays, by invoking the concept of ray/mode duality. The criterion for a ray to correspond to a mode is given. Each ray path undergoes curvature in the horizontal direction, or horizontal refraction, due to the multiple acoustic interactions with the inclined boundaries of the wedge, and the rays corresponding to a given mode are found to be constrained to fall precisely within the modal beam. From simple geometric arguments, these modal rays cannot extend beyond the beam, and shadow zones are formed.</p>				
20. DISTRIBUTION/AVAILABILITY OF ABSTRACT UNCLASSIFIED/UNLIMITED <input checked="" type="checkbox"/> SAME AS RPT. <input type="checkbox"/> DTIC USERS <input type="checkbox"/>		21. ABSTRACT SECURITY CLASSIFICATION <b>UNCLASSIFIED</b>		
22a. NAME OF RESPONSIBLE INDIVIDUAL Michael J. Buckingham		22b. TELEPHONE NUMBER (Include Area Code) 202 767-2307	22c. OFFICE SYMBOL Code 5121	

DD FORM 1473, 83 APR

EDITION OF 1 JAN 73 IS OBSOLETE.

SECURITY CLASSIFICATION OF THIS PAGE

11. TITLE (Include Security Classification) (Continued)

**ACOUSTIC PROPAGATION IN A WEDGE-SHAPED OCEAN  
WITH PERFECTLY REFLECTING BOUNDARIES**

16. Supplementary Notation (Continued)

The material contained in this report was presented in A.B. Wood Memorial Lecture, which was delivered at the Institute of Acoustics Conf. Acoustics and the Sea Bed, Univ. of Bath, UK, 6-8 Apr. 1983. The author is an exchange scientist from the Royal Aircraft Establishment, Farnborough, Hants, GU14 6TD, England.

## CONTENTS

INTRODUCTION .....	1
THE FIELD DUE TO A POINT SOURCE IN THE WEDGE .....	1
THE NORMAL MODE INTEGRAL .....	4
THE EIGENFUNCTIONS FOR THE WEDGE .....	5
TOTAL NUMBER OF MODES IN THE FIELD .....	6
SPATIAL PROPERTIES OF THE MODES .....	8
Range Dependence of the Modes ( $z = 0$ ) .....	8
Z-Dependence of the Modes .....	9
RAY/MODE DUALITY .....	12
EXPERIMENTAL EVIDENCE .....	14
CONCLUDING REMARKS .....	15
ACKNOWLEDGMENTS .....	16
REFERENCES .....	16
APPENDIX A—Evaluation of the Normal Mode Integral .....	17
APPENDIX B—The Field in the Vicinity of the Source .....	19
APPENDIX C—Mode/Ray Hyperbolae .....	22



# ACOUSTIC PROPAGATION IN A WEDGE-SHAPED OCEAN WITH PERFECTLY REFLECTING BOUNDARIES

## INTRODUCTION

The ocean overlying the continental slope or a sloping beach is most simply represented as a wedge-shaped domain with perfectly reflecting (pressure-release) boundaries. This model is, of course, inadequate in that it cannot account for certain phenomena, such as acoustic penetration of the bottom, which are encountered in the real ocean. On the other hand, the wave equation for the perfect wedge is separable, and the analysis of the acoustic field due to a point source within the domain is tractable. By way of contrast, the wave equation for the penetrable wedge is not separable, a fact which inevitably complicates the analysis of the acoustic field in this case. Here we shall confine our attention to the simpler situation where the boundaries are perfect reflectors. Certain physical attributes of the perfect wedge are discussed, most notably the fact that the radiation field is constrained to form modal beams as a result of the multiple acoustic interactions with the boundaries. This conclusion, which derives from the solution of the wave equation, can be most satisfactorily interpreted by calling on the concept of ray/mode duality. The question of the connection between rays and modes in the wedge is pursued here at some length.

In general, the radiation field in a wedge-shaped domain formed by two perfectly reflecting boundaries consists of two components: the modal component is a consequence of the constraints imposed by the boundary planes on the field, and the diffracted component arises from scattering at the apex of the wedge. It is well known [1] that when the wedge angle is a submultiple of  $\pi$ , the diffracted component is identically zero; and in certain special cases, even when the wedge angle is not a submultiple of  $\pi$ , the diffracted component is again absent [2]. What is more significant, however, is that in the context of ocean wedges, where the wedge angle is usually very small (typically a few degrees) and the ranges of the source and the receiver from the apex are generally many wavelengths long, the diffracted component, if not absent, is negligibly small. This being so, it is ignored in the following discussion, which is devoted to the modal component of the field.

An approximate solution for the modal part of the field in a perfect wedge has been derived by Bradley and Hudimac [3] and examined by Graves et al. [4]. Unfortunately, its range of validity is extremely limited. In particular, it is unsatisfactory throughout a large proportion of the modal beams alluded to above, in just the regions which are of interest in many applications. The failure of Bradley and Hudimac's solution in these regions could, perhaps, have been anticipated, since it does not show the required form around the source point. One of the main results in the present report is a new solution for the field in the wedge, which has a much more extensive range of validity than that of Bradley and Hudimac, and which behaves correctly in the immediate vicinity of the source.

## THE FIELD DUE TO A POINT SOURCE IN THE WEDGE

The geometry for the wedge problem is shown in Fig. 1, where  $S$  and  $R$  represent a point source and a point receiver, respectively. Since we are interested in the three-dimensional field in the wedge,  $S$  and  $R$  are not necessarily in the same vertical plane running perpendicular to the apex of the wedge. The angle of the wedge is  $\theta_0$ . A cylindrical coordinate system is used for the problem, with the  $z$  axis running down the apex of the wedge and the angular coordinate  $\theta$  measured from the surface. Thus the boundary planes are at  $\theta = 0$  and  $\theta = \theta_0$ . The coordinates of the receiver are  $(r, \theta, z)$  and those of the source, which for convenience is located in the  $z = 0$  plane, are the primed quantities  $(r', \theta', 0)$ .

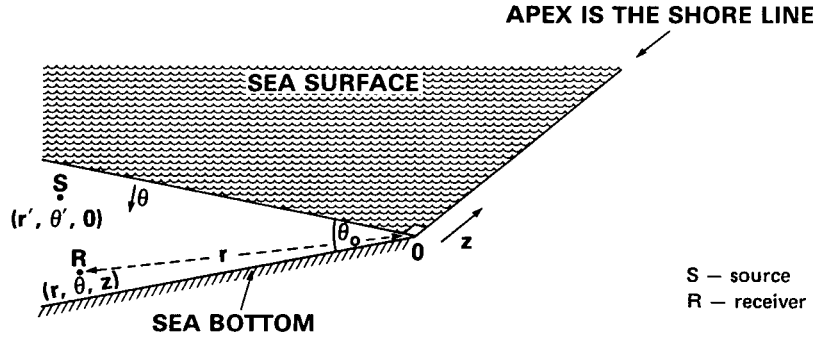


Fig. 1 - Cylindrical coordinate system for the wedge problem

The equation that must be solved for the field in the wedge is the inhomogeneous Helmholtz equation:

$$\nabla^2 \phi + k^2 \phi = -Q \frac{\delta(r-r')}{r} \delta(\theta-\theta') \delta(z), \quad (1)$$

where  $Q$  is the source strength,  $\delta(\cdot)$  is the Dirac delta function, and  $k$  is the wavenumber (i.e.,  $k = \omega/c$ , where  $\omega$  is the angular frequency and  $c$  is the speed of sound in the medium, which is assumed to be independent of position). The function  $\phi$  in Eq. (1) is the velocity potential excluding the time-dependent factor in the case of an harmonic source, or it is the Fourier transform (with respect to time) of the velocity potential for an impulsive source. On expressing the Laplacian operator in cylindrical coordinates, Eq. (1) becomes

$$\frac{1}{r} \frac{\partial}{\partial r} \left( r \frac{\partial \phi}{\partial r} \right) + \frac{1}{r^2} \frac{\partial^2 \phi}{\partial \theta^2} + \frac{\partial^2 \phi}{\partial z^2} + k^2 \phi = -Q \frac{\delta(r-r')}{r} \delta(\theta-\theta') \delta(z). \quad (2)$$

Equation (2) is separable for the perfect wedge, and it can be solved for  $\phi$  in several ways. The method used here is to apply a sequence of integral transforms to both sides, and subsequently to apply the inverse transforms to arrive at the solution. Assuming pressure-release boundaries, the first of these transforms is the finite Fourier sine transform:

$$\phi_s = \int_0^{\theta_0} \phi(\theta) \sin \nu \theta d\theta, \quad (3a)$$

whose inverse is

$$\phi(\theta) = \frac{2}{\theta_0} \sum_{\nu} \phi_s(\nu) \sin \nu \theta. \quad (3b)$$

In these expressions,  $\nu = m\pi/\theta_0$ , where  $m$  is a positive integer, and the symbol  $\Sigma_{\nu}$  means a sum over all possible values of  $m$ . It is clear from the structure of Eq. (3b) that the final solution for the field will be a sum of normal modes, and that  $m$  is the mode number. Note also that this formulation ensures that the pressure-release boundary conditions are satisfied. On taking the sine transform of Eq. (2), we obtain

$$\frac{1}{r} \frac{\partial}{\partial r} \left( r \frac{\partial \phi_s}{\partial r} \right) - \frac{\nu^2}{r^2} \phi_s + \frac{\partial^2 \phi_s}{\partial z^2} + k^2 \phi_s = -Q \frac{\delta(r-r')}{r} \delta(z) \sin \nu \theta'. \quad (4)$$

The next transform to apply is the generalized Hankel transform of order  $\nu = m\pi/\theta_0$ , which we shall assume to be an integer. This is tantamount to saying that  $\theta_0$  is a submultiple of  $\pi$ , so that the field due to diffraction at the apex of the wedge is zero. The Hankel transform is defined as

$$H_\nu(\phi_s) \equiv \phi_{\nu,s} = \int_0^\infty r \phi_s(r) J_\nu(pr) dr, \quad (5a)$$

and the inverse transform is

$$\phi_s(r) = \int_0^\infty p \phi_{\nu,s}(p) J_\nu(pr) dp. \quad (5b)$$

An important property of the Hankel transform is that it acts on the quantity  $\Delta_\nu \phi_s$  as follows [5]:

$$H_\nu(\Delta_\nu \phi_s) = -p^2 H_\nu(\phi_s), \quad (6a)$$

where  $\Delta_\nu$  is the differential operator

$$\Delta_\nu = \left\{ \frac{1}{r} \frac{\partial}{\partial r} \left[ r \frac{\partial}{\partial r} \right] - \frac{\nu^2}{r} \right\}. \quad (6b)$$

Thus, when Eq. (4) is Hankel transformed we find that

$$\frac{\partial^2 \phi_{\nu,s}}{\partial z^2} + (k^2 - p^2) \phi_{\nu,s} = -Q \sin \nu \theta' J_\nu(pr') \delta(z). \quad (7)$$

The final transformation to apply is the Laplace transform, defined as

$$\phi_{l,\nu,s} = \int_0^\infty \phi_{\nu,s}(z) \exp(-qz) dz, \quad (8)$$

where the unilateral form has been chosen because the field must be symmetrical in  $z$ . On applying this integral transformation to Eq. (7), we find that

$$\phi_{l,\nu,s} = \frac{q \phi_{\nu,s}(0) - \frac{Q}{2} \sin \nu \theta' (J_\nu(pr'))}{(q^2 + k^2 - p^2)}, \quad (9)$$

where  $\phi_{\nu,s}(0)$  is the value of  $\phi_{\nu,s}$  at  $z = 0$ . Now, the inverse Laplace transform of Eq. (9) is easily shown to be

$$\phi_{\nu,s} = \phi_{\nu,s}(0) \cos \eta |z| - \frac{Q}{2} \sin \nu \theta' J_\nu(pr') \frac{\sin \eta |z|}{\eta}, \quad (10)$$

where

$$\eta = \sqrt{k^2 - p^2}. \quad (11)$$

From the radiation condition, that is, the requirement that the field should go to zero when  $|z| \rightarrow \infty$  for  $p > k$ , we find that

$$\phi_{\nu,s}(0) = j \frac{Q}{2} \sin \nu \theta' \frac{J_\nu(pr')}{\eta}, \quad (12)$$

and hence

$$\phi_{\nu,s} = j \frac{Q}{2} \sin \nu \theta' \frac{J_\nu(pr')}{\eta} \exp(j \eta |z|). \quad (13)$$

The next inversion integral to apply is the inverse Hankel transform defined in Eq. (5b). Using the expression in Eq. (13), this gives

$$\phi_s = j \frac{Q}{2} \sin \nu \theta' \int_0^\infty \frac{p \exp(j \eta |z|) J_\nu(pr) J_\nu(pr')}{\eta} dp. \quad (14)$$

Finally, we obtain the solution for the field in the wedge by taking the inverse sine transform of  $\phi_s$  defined in Eq. (3b):

$$\phi = \frac{Q}{\theta_0} \sum_\nu I_\nu(r, r', z) \sin \nu \theta \sin \nu \theta'. \quad (15)$$

This is a sum of normal modes whose coefficients are given by the integral

$$I_\nu(r, r', z) = j \int_0^\infty p \frac{\exp(j\eta|z|)}{\eta} J_\nu(pr) J_\nu(pr') dp. \quad (16)$$

Note that the solution as it stands in Eq. (15) is exact, since no approximations have yet been introduced. It is only in evaluating  $I_\nu$  that some accuracy will be sacrificed.

### THE NORMAL MODE INTEGRAL

To evaluate the integral in Eq. (16), it is convenient to convert it to another form using the Bessel function identity [6]

$$J_\nu(pr) J_\nu(pr') = \frac{1}{\pi} \int_0^\pi J_0(p \sqrt{r^2 + r'^2 - 2rr' \cos \sigma}) \cos \nu \sigma d\sigma, \quad (17)$$

which is valid for  $\nu$  an integer. When this expression is substituted into Eq. (16), we obtain the double integral

$$I_\nu = \frac{j}{\pi} \int_0^\pi \cos \nu \sigma \int_0^\infty p \frac{\exp(j\eta|z|)}{\eta} J_0(p \sqrt{r^2 + r'^2 - 2rr' \cos \sigma}) dp d\sigma. \quad (18)$$

Now, the inner integral here is the field due to a point source in an infinite medium [7], and hence  $I_\nu$  can be written as

$$I_\nu = \frac{1}{\pi R_0} \int_0^\pi \cos \nu \sigma \frac{\exp[-jkR_0(1 - 2a \cos \sigma)^{1/2}]}{(1 - 2a \cos \sigma)^{1/2}} d\sigma, \quad (19)$$

where

$$R_0 = (r^2 + r'^2 + z^2)^{1/2}, \quad a = \frac{rr'}{R_0^2} \leq 1/2. \quad (20)$$

From the definitions in Eq. (20), it is clear that  $a$  takes its maximum value, equal to 1/2, when  $r = r'$  and  $z = 0$ . As the source and receiver separate in the  $r - z$  plane,  $a$  falls in value, approaching zero in the limit.

The form of the integral in Eq. (19) is more amenable to evaluation by approximation techniques than is the form in Eq. (16). An evaluation procedure is described in Appendix A which leads to the result

$$I_\nu = \frac{1}{2} \exp j \frac{\nu \pi}{2} \left[ \frac{\exp\{-jkR_1(1 + b_1)\} H_\nu^{(1)}(kR_1 b_1)}{R_1} + \frac{\exp\{-jkR_2(1 - b_2)\} H_\nu^{(2)}(kR_2 b_2)}{R_2} \right], \quad (21a)$$

which is valid provided the condition

$$kR_0 a \gg 1 \quad (21b)$$

is satisfied. In the expression for  $I_\nu$  in Eq. (21a),  $H_\nu^{(1)}()$  and  $H_\nu^{(2)}()$  are Hankel functions of order  $\nu$  of the first and second kind, respectively, and the parameters  $R_i$  and  $b_i$ ,  $i = 1, 2$  are defined as follows:

$$R_1 = R_0(1 - 2a)^{1/2}, \quad R_2 = R_0(1 + 2a)^{1/2}, \quad b_1 = \frac{a}{(1 - 2a)}, \quad b_2 = \frac{a}{(1 + 2a)}. \quad (22)$$

Notice that, apart from  $\nu$ , the formulation of  $I_\nu$  given above depends on only two independent variables, namely  $kR_0$  and  $a$ . Equations (15) and (21) specify the modal field in the wedge.

In the context of ocean wedges, where the wedge angle is usually substantially less than  $10^\circ$ , the inequality in Eq. (21b) does not represent a serious practical restriction on the validity of the solution for  $I_\nu$ . As we shall demonstrate, each mode in the wedge takes the form of a beam of radiation which diverges as the range from the apex increases. Within, and to some extent beyond, a modal beam, the condition in Eq. (21b) is always satisfied. It is only deep within those regions which are not illuminated by the source, that is to say, the acoustic shadow zones, that, Eq. (21b) may not hold, but this is not a significant limitation because the field in these regions is essentially zero anyway. We conclude, therefore, that Eq. (21a) is a valid description of the modes for most scenarios appropriate to the ocean wedge.

It is worth noting in particular that Eq. (21a) is a valid representation of the field in the immediate vicinity of the source point (assuming that the source is many wavelengths from the apex so that equation (21b) is satisfied). Under these circumstances it can be shown that the mode sum for the field in the wedge reduces to the free-field expression for a point source (see Appendix B). This is exactly the form of limiting behavior that is required of the solution.

It is interesting to examine Eq. (21a) in another limit, in this case as  $a \rightarrow 0$ , corresponding to a large separation between the source and the receiver in the  $r-z$  plane. In this limit, we have  $R_1 = R_2 = R_0$  and  $b_1 = b_2 = a$ , which, when substituted into Eq. (21a) give

$$\lim_{a \rightarrow 0} I_\nu = \frac{1}{R_0} \exp \left\{ j \frac{\nu\pi}{2} \right\} \exp -(jkR_0) J_\nu(kR_0 a), \quad (23)$$

where the sum of the two Hankel functions has been expressed as a Bessel function of the first kind. This expression is the solution for the modal coefficients that was obtained by Bradley and Hudimac [3]. Naturally, its range of validity is considerably less than that of the solution in Eq. (21a), since the additional constraint  $a = 0$  has now to be satisfied. This condition means that Eq. (23) is not a valid representation of the field in the vicinity of the source, as exemplified by the fact that it does not show the required singularity at the source point.

The implications of the condition  $a = 0$  are well illustrated by an example. If we assume that  $a \leq 0.1$ , and that the source and the receiver are in the same vertical plane perpendicular to the apex so that  $z = 0$ , then a simple calculation shows that Eq. (23) is valid only when  $r \leq r'/10$  or when  $r \geq 10r'$ . Taking the range of the source from the apex as 1 km, say, this means that Eq. (23) is invalid for all receiver ranges (measured from the apex) between 100 m and 10 km. It is unfortunate, in view of the relative simplicity of Eq. (23), that this is precisely the range that is likely to be of interest in practical situations.

An impression of the relative accuracies of Eqs. (21a) and (23) is conveyed by Table 1, which shows the real part, the imaginary part, and the modulus of the quantity  $\pi R_0 I_\nu$  for various values of  $a$  and  $kR_0$ , but chosen so that the product  $kR_0 a = 100$ . For comparison, a numerically computed evaluation of the integral in Eq. (19) is included in the table. The agreement between Eq. (21a) and the computed values is apparent. Equation (23), on the other hand, performs poorly, especially with regard to phase. This is true even when  $a$  takes the relatively low value of 0.1 used in the example cited above. An improvement occurs only when  $a$  is substantially less than 0.1, confirming that Eq. (23) has an extremely limited range of validity.

## THE EIGENFUNCTIONS FOR THE WEDGE

The trigonometric functions in Eq. (15) contain the entire angular dependence of the modes in the perfect wedge. These oscillatory functions are analogous to the eigenfunctions obtained for a shallow-water channel with pressure-release boundaries. In the shallow water case, the variable is the depth of the sensor or the source, normalized to the channel depth, whereas in the wedge it is the angular depth normalized to the wedge angle.

Table 1 — The Modal Coefficients for  $\nu = 18$  (corresponding to the first mode in a  $10^\circ$  wedge)

$a$	$kR_0$	$\Re e(\pi R_0 I_\nu)$	$\Im m(\pi R_0 I_\nu)$	$R_0 \pi  I_\nu $	Footnote
$10^{-4}$	$10^6$	0.225	0.085	0.241	<sup>a</sup>
		0.225	0.085	0.241	<sup>b</sup>
		0.226	0.084	0.241	<sup>c</sup>
0.1	$10^3$	-0.118	-0.131	0.176	<sup>a</sup>
		-0.119	-0.132	0.178	<sup>b</sup>
		0.136	-0.199	0.241	<sup>c</sup>
0.2	500	-0.192	-0.042	0.197	<sup>a</sup>
		-0.193	-0.042	0.198	<sup>b</sup>
		-0.213	-0.113	0.241	<sup>c</sup>
0.4	250	-0.025	0.244	0.245	<sup>a</sup>
		-0.025	0.245	0.246	<sup>b</sup>
		0.058	0.234	0.241	<sup>c</sup>
0.4975	201	-0.413	-0.400	0.574	<sup>a</sup>
		-0.403	-0.409	0.574	<sup>b</sup>
		0.241	0.015	0.241	<sup>c</sup>

<sup>a</sup>Numerical evaluation of the integral in Eq. (17).

<sup>b</sup>Evaluation of the new analytical solution in Eq. (21a).

<sup>c</sup>Evaluation of Bradley and Hudimac's solution in Eq. (23).

The function  $\sin(m\pi\theta/\theta_0)$  is plotted for the first three modes, corresponding to  $m = 1, 2, 3$ , in Fig. 2. Note that each mode is zero on the boundaries, and that the  $m$ th mode exhibits  $m$  extrema.

### TOTAL NUMBER OF MODES IN THE FIELD

The integral for  $I_\nu$  in Eq. (19) is essentially zero when  $\nu$  exceeds a certain value. This can be appreciated by allowing  $\nu$  to become indefinitely large, in which case the trigonometric function oscillates far more rapidly than the rest of the integrand. If the slowly varying part, that is, everything except the cosine, is treated as a constant and taken outside the integral, then the integral of the cosine function is identically zero (bearing in mind that  $\nu = m\pi/\theta_0$ , and we are assuming that  $\theta_0$  is a submultiple of  $\pi$ ). The implication of this is that only a finite number  $M$  of modes contributes significantly to the field at any point in the wedge.

To estimate  $M$ , we set

$$\mu(\sigma) = kR_0(1 - 2a \cos \sigma)^{1/2} \tag{24}$$

and employ the condition that the integral in Eq. (19) takes appreciable values only when

$$\nu = \frac{m\pi}{\theta_0} \leq \left. \frac{d\mu}{d\sigma} \right|_{\max} \tag{25}$$

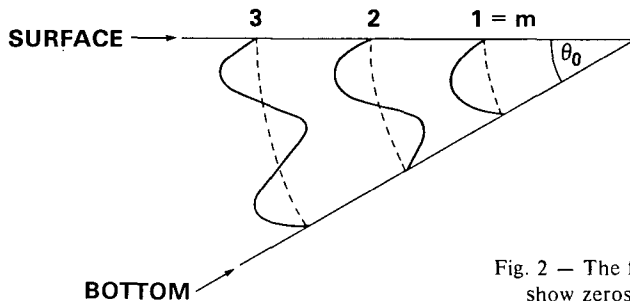


Fig. 2 — The first three mode shapes in the wedge. All show zeros on the (pressure-release) boundaries.

where  $(d\mu/d\sigma)|_{\max}$  is the maximum 'frequency' of the exponential term in the integrand. A simple calculation shows that

$$\left. \frac{d\mu}{d\sigma} \right|_{\max} = \frac{kR_0}{\sqrt{2}} \{1 - (1 - 4a^2)^{1/2}\}^{1/2}. \quad (26)$$

Thus, the maximum value of  $m$  from Eq. (25) is

$$M = E \left[ \frac{kR_0\theta_0}{\pi\sqrt{2}} \{1 - (1 - 4a^2)^{1/2}\}^{1/2} \right], \quad (27)$$

where the symbol  $E[ ]$  denotes "integer part of."

It is apparent from Eq. (27) that  $M$ , the total number of propagating modes at the receiver, depends on the positions of the source and the receiver. There are two cases in particular which are worth noting.

Case 1. Source and receiver coincident in  $r - z$  plane ( $a = 1/2$ )

In this configuration, we have  $r = r'$  and  $z = 0$ , giving  $R_0 = \sqrt{2} r'$ , and from Eq. (27)

$$M = E \left[ \frac{kr'\theta_0}{\pi} \right]. \quad (28)$$

Thus the total number of modes in this case is governed by the water depth  $r'\theta_0$  at the source.

Case 2. Source and receiver well separated in range and/or  $z$  ( $a \rightarrow 0$ )

In this case, the right-hand side of Eq. (26) becomes equal to  $kR_0a$ , and the expression in Eq. (27) for  $M$  reduces to

$$M = E \left[ \frac{kR_0\theta_0a}{\pi} \right] = E \left[ \frac{krr'\theta_0}{\pi(r^2 + r'^2 + z^2)^{1/2}} \right]. \quad (29)$$

In certain specific situations, this may be simplified further, as follows:

$$M = E \left[ \frac{kr\theta_0}{\pi} \right] \text{ when } r' \gg r, z = 0, \quad (30a)$$

$$M = E \left[ \frac{kr'\theta_0}{\pi} \right] \text{ when } r \gg r', z = 0, \quad (30b)$$

and

$$M = E \left[ \frac{krr'\theta_0}{\pi|z|} \right] \text{ when } |z| \gg r \text{ and } |z| \gg r'. \quad (30c)$$

Equations (30a) and (30b) correspond to the receiver being upslope and downslope of the source, respectively. In both cases, the total number of modes is governed by the water depth ( $r\theta_0$  or  $r'\theta_0$ ) at the shallower location. Moreover, Eqs. (30a) and (30b) are the same results that would have been obtained from shallow water theory, had we assumed that the bottom was locally flat at  $r$  and  $r'$ , respectively. (A similar statement applies to Eq. (28)).

**SPATIAL PROPERTIES OF THE MODES**

As the solution for the acoustic field has the angular dependence separated out, the behavior of the modes in the range and  $z$  directions can be discussed independently of their angular properties. To examine this behavior, we should strictly employ the expression for  $I_\nu$  in Eq. (21a). (In certain applications, for example in determining the response of an array of sensors in a wedge-shaped channel where phase is of critical importance, this would be essential.) However, we are interested here only in establishing the broad features of the field, and for this purpose the simpler expression in Eq. (23) is adequate. In particular we shall focus attention on the Bessel function  $J_\nu(kR_0a)$ , since this contains most of the interesting properties of the field; the exponential functions merely influence the phase of the field, and  $R_0$  in the denominator is only a spreading term.

**Range-Dependence of the Modes ( $z = 0$ )**

We begin by considering upslope propagation, with the source much further from the apex of the wedge than the receiver (i.e.,  $r' \gg r$ ), and with the source and the receiver in the same vertical plane perpendicular to the apex (i.e.,  $z = 0$ ). Under these conditions, the Bessel function in Eq. (23) can be expressed simply as  $J_\nu(kr)$ . This function is plotted in Fig. 3 for  $\nu = 18, 36,$  and  $54$ , corresponding to the first three modes in a  $10^\circ$  wedge. The vertical arrows are at the mode cutoff points calculated from shallow water theory. The curves are highly oscillatory beyond some cutoff value of  $kr$ , which increases with the mode number. Below cutoff (i.e., for smaller values of  $kr$ ) the modal field falls rapidly to zero and remains there right up to the apex. Immediately above cutoff, the mode envelope is a maximum, and it decays approximately as  $(kr)^{-1/2}$  as  $kr$  rises.

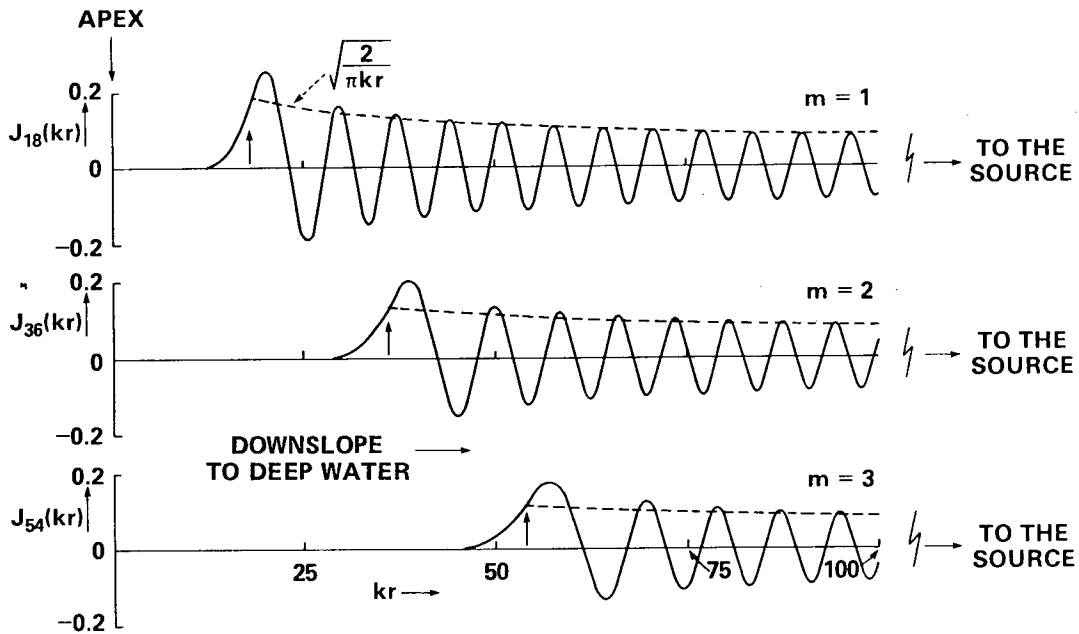


Fig. 3 — The mode amplitude function  $J_\nu(kr)$  for  $\nu = 18, 36,$  and  $54$

By examining the series expansion

$$J_\nu(x) = \frac{(x/2)^\nu}{\nu!} \left[ 1 - \frac{(x/2)^2}{(\nu+1)} + \dots \right] \quad (31)$$

for the Bessel function of integer order  $\nu$ , it can easily be seen from the term outside the square brackets that, for large  $\nu$ ,  $J_\nu(x)$  drops extremely rapidly to zero when the argument  $x$  falls below the order

$\nu$ . Taking equality between  $x$  and  $\nu$  as the condition for the onset of this behavior (i.e., when  $x \leq \nu$ ,  $J_\nu(x) = 0$ ), we can define for the  $m$ th mode the cutoff range from the apex,  $r_{cm}$ , as

$$kr_{cm} = m\pi/\theta_0. \tag{32}$$

This result is equivalent to that in Eq. (30a), derived from considerations of the mode integral.

The vertical arrows in Fig. 3 indicate the cutoff points for the three modes, calculated from Eq. (32). If  $r_{cm} \theta_0$  is equated with the water depth at the cutoff range, then Eq. (32) is the same as that obtained from shallow water theory for mode cutoff. The obvious physical interpretation of this is that if the wedge is regarded as being locally uniform in depth, then at ranges less than  $r_{cm}$  the channel is not sufficiently deep to support the  $m$ th mode.

A qualitative interpretation of the curves in Fig. 3 can be given in terms of rays (Fig. 4). A ray travelling upslope undergoes numerous reflections from the boundary planes, increasing its grazing angle on successive bounces from either one of the planes by twice the wedge angle. Eventually, as the apex is approached, the grazing angle becomes so large that the ray is turned around and proceeds to propagate back downslope. In the vicinity of the turnaround point, which corresponds closely to the mode cutoff range given by Eq. (32), the density of rays is high, which is consistent with the relatively high level of the modal envelope immediately above cutoff.

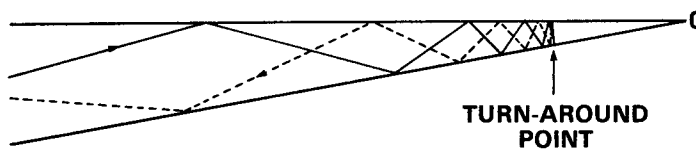


Fig. 4 — A ray propagating upslope is eventually turned around and then propagates back downslope

**Z-Dependence of the Modes**

The argument of the mode amplitude function  $J_\nu(kR_0a)$  depends on  $z$  (the separation of the source and receiver in the direction parallel to the apex) through the term  $R_0$  (see definition in Eq. (20)). We now examine this  $z$ -dependence downslope of the source with the ranges of the source and the receiver held fixed. Fig. 5 shows the function

$$J_{18} \left\{ \frac{krr'}{(r^2 + r'^2 + z^2)^{1/2}} \right\}$$

corresponding to the first mode in a 10° wedge, plotted as a function of  $z$ , assuming that  $r \gg r'$ . Note that when  $|z|$  exceeds a certain critical value the field falls to zero, and where it is nonzero it is highly oscillatory suggesting strong interference. The envelope of the oscillatory function, derived from the asymptotic expansion of the Bessel function, is shown as the broken line, with the cutoff points in  $|z|$  determined as in Eq. (32), by equating the argument with the index. The resemblance of this outline to a butterfly with spread wings is apparent, which suggests the term "modal butterfly." The wingspan is clearly dependent on the mode number, as illustrated in Fig. 6 for the first four modal butterflies of a 10° wedge. As the mode number increases, it is evident that the width of the nonzero field region in the  $z$ -direction becomes narrower, eventually cutting off altogether above some value of  $m$  depending on the local conditions. The criterion governing the number of propagation modes at any given point has already been established and is given in Eq. (27).

The significance of the modal butterflies becomes apparent when the wingspan is examined as a function of range. This is shown for the first mode in Fig. 7. The radiation field diverges from the

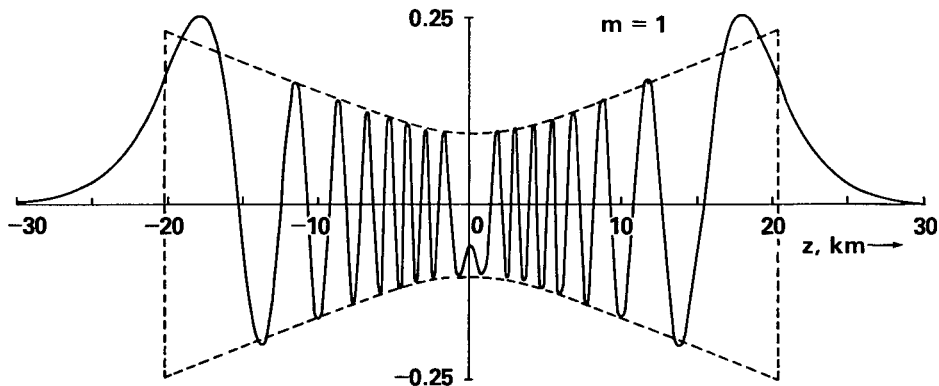


Fig. 5 —  $z$ -dependence of the first mode at a fixed range 5 km downslope of the source, which is located in the  $z = 0$  plane ( $\theta_0 = 10^\circ$ )

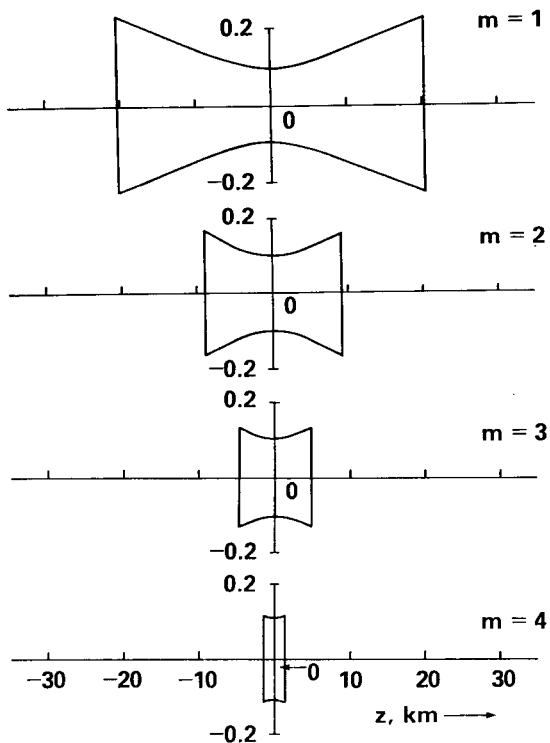
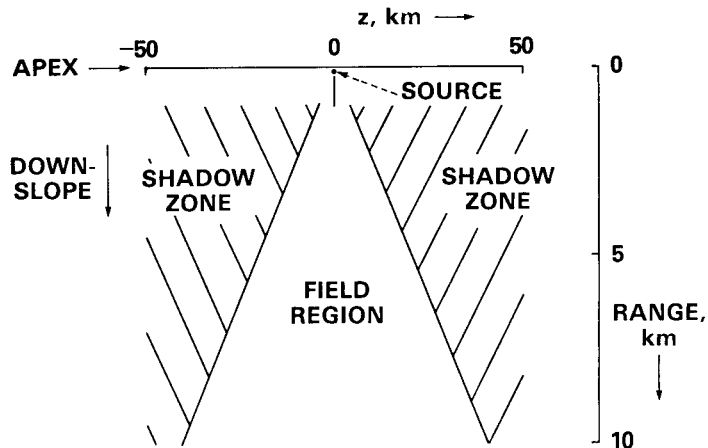


Fig. 6 — The first four modal butterflies at a fixed range 5 km downslope of the source, which is located in the  $z = 0$  plane ( $\theta_0 = 10^\circ$ )

Fig. 7 — Range-dependence of the wingspan downslope of the source. Outside the beam the field decays rapidly to form shadow zones ( $\theta_0 = 10^\circ$ ).



source to illuminate a fan-like region beyond which there is essentially no energy, and acoustic shadow zones are formed. Thus, the interaction of the radiation with the boundaries creates a beaming effect. In practical situations this could be important since regions of the ocean are not being ensonified. Figure 8 shows the same phenomenon for the first four modes, and clearly illustrates the nested structure of the modal beams—as the mode number rises, the width of the beam decreases, which is consistent with the argument given above for the behavior of the wingspan with mode number.

A similar situation is encountered with the field upslope of the source, except that in this case the field converges as the receiver recedes from the source (i.e., as the shoreline is approached). This is illustrated in Fig. 9 for the first mode. The beam shape is hyperbolic [8], as is easily confirmed from the mode amplitude Bessel function. The beams corresponding to the higher order modes again fall within those of the lower order modes, although this is not shown in Fig. 9. As before, outside a given beam there is essentially no energy in the field associated with that particular mode. Thus, the maximum extent of the ensonified region in the  $|z|$  direction is determined by the lowest order mode in the field.

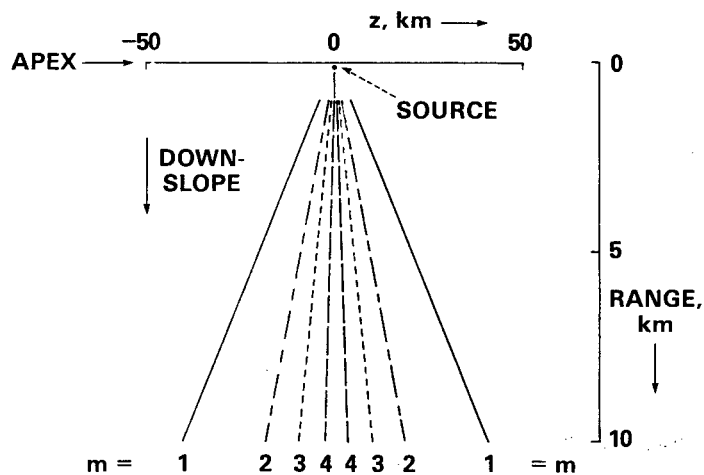


Fig. 8 — The first four modal beams, showing their nested structure

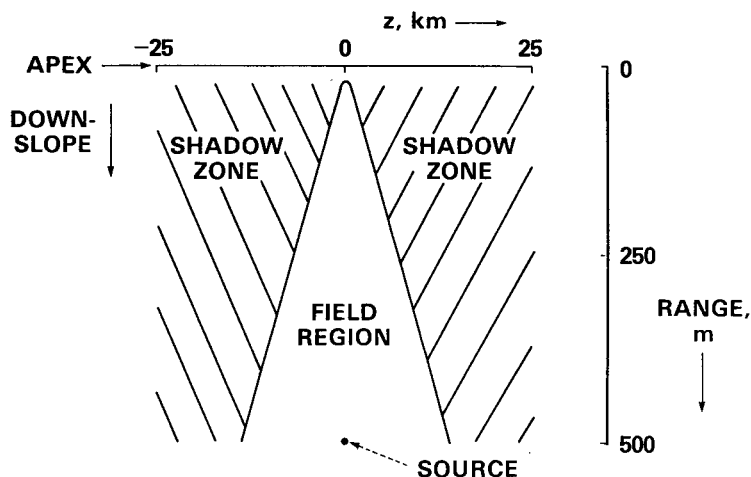


Fig. 9 — The field and shadow zones of the first mode upslope of the source. The boundary curve is a hyperbola ( $\theta_0 = 10^\circ$ ).

## RAY/MODE DUALITY

Each mode in the wedge is a superposition of two components, represented by the two terms containing the Hankel functions in Eq. (21a). When the arguments of these functions are very much greater than the order  $\nu$ , the Hankel functions themselves may be approximated by their asymptotic forms. The range dependence of the two modal field terms is then given by the oscillatory functions  $\exp(-jkR_1)$  and  $\exp(-jkR_2)$ , where from the definitions in Eqs. (20) and (22), we see that

$$R_1 = [(r - r')^2 + z^2]^{1/2}, \quad R_2 = [(r + r')^2 + z^2]^{1/2}. \quad (33)$$

These expressions show that, in the  $(r, z)$  plane,  $R_1$  is the range from the source to the receiver, and  $R_2$  is the range from an image source at  $(-r', 0)$  to the receiver. Thus, in the asymptotic region the two exponential functions are representative of two sets of waves, one of which is produced by the source and the other of which is associated with the image.

The appearance of the two field components in the modal solution can be understood by examining a ray path in the wedge, or more precisely, the horizontal projection of a ray onto the sea surface as it bounces between the surface and the bottom. Weston [9] has discussed this device and has shown from geometrical arguments that the shape of the horizontally projected ray path is a hyperbola (Fig. 10). That is, the repeated acoustic interactions with the inclined planes forming the wedge introduce a curvature into the horizontal direction of travel of the ray and eventually lead to a turning point as the shoreline is approached. (Weston refers to this phenomenon as horizontal refraction.) If the asymptote associated with the branch of the hyperbola remote from the source is extended beyond the apex, it passes through the image source at  $(-r', 0)$ .

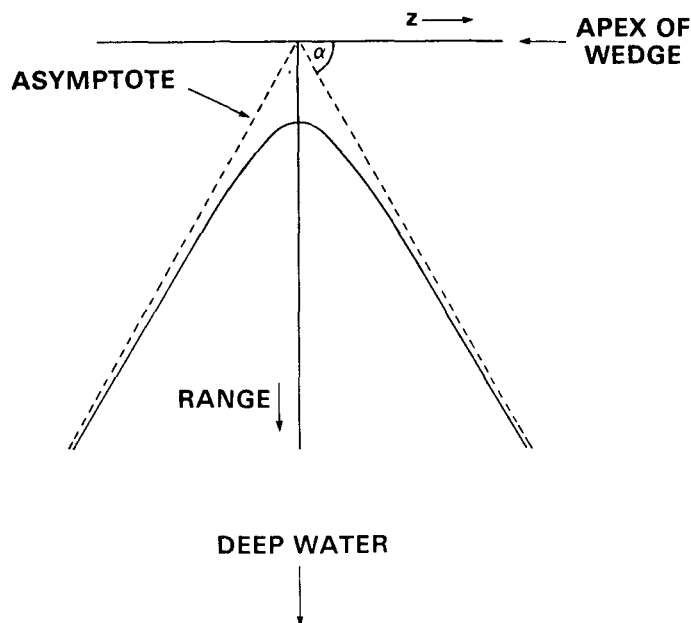


Fig. 10 — Horizontal projection of a ray path in the wedge

There are many possible hyperbolic ray paths between a source and a receiver in the wedge. Most of these do not show constructive interference and hence do not correspond to a mode. The criterion for a ray to correspond to the  $m$ th mode is that *the grazing angle of the ray at the vertex of its hyperbolic path must be the same as that of the ray corresponding to the  $m$ th mode in shallow water whose depth is equal*

to the depth at the vertex. Weston [9] has shown that the angle between the asymptotes of a hyperbolic ray path and the shoreline is the same as the grazing angle at the vertex. It follows that the criterion given above for a ray to correspond to a mode fixes the directions of the arms of the modal hyperbola. This is an important factor in interpreting the modal beams and shadow zones in the wedge.

The quantity

$$T = \int_0^h \frac{\sin \alpha}{c} dh, \tag{34a}$$

where  $h$  is the water depth and  $\alpha$  is the grazing angle, is a ray invariant [10]. For isovelocity water (which is our case),  $\alpha$  and  $c$  are independent of depth, and so

$$T = \frac{h \sin \alpha}{c}. \tag{34b}$$

Thus, in the wedge the quantity in Eq. (34b) is a constant along the hyperbolic ray path. But the condition for a ray to correspond to a mode in a shallow water channel with pressure-release boundaries is

$$h \sin \alpha = \frac{m\pi}{k} = \text{const.} \tag{35}$$

On comparing these two expressions, it can be deduced that in the wedge a hyperbolic ray corresponding to a mode behaves as though it were a mode in locally shallow water all along its track. That is, at each point along the hyperbolic path, the upward and downward traveling wavefronts obey the same conditions for constructive interference as if the channel were locally uniform in depth.

For a fixed source/receiver configuration in the wedge, there are only two possible modal rays corresponding to the  $m$ th mode. They are illustrated in Fig. 11. (The parameters of these hyperbolae are easily expressed in terms of  $r$ ,  $r'$ ,  $z$ ,  $m$ , and  $\theta_0$  from a geometrical argument, as detailed in Appendix C). One is a direct ray from the source and the other is an indirect ray, which has been turned around on approaching the apex, as shown in the figure. When the receiver is in the asymptotic regions of these two hyperbolic ray paths, the direct and indirect rays correspond to the field terms from the source and its image, respectively, in the modal solution (Eq. (21a)).

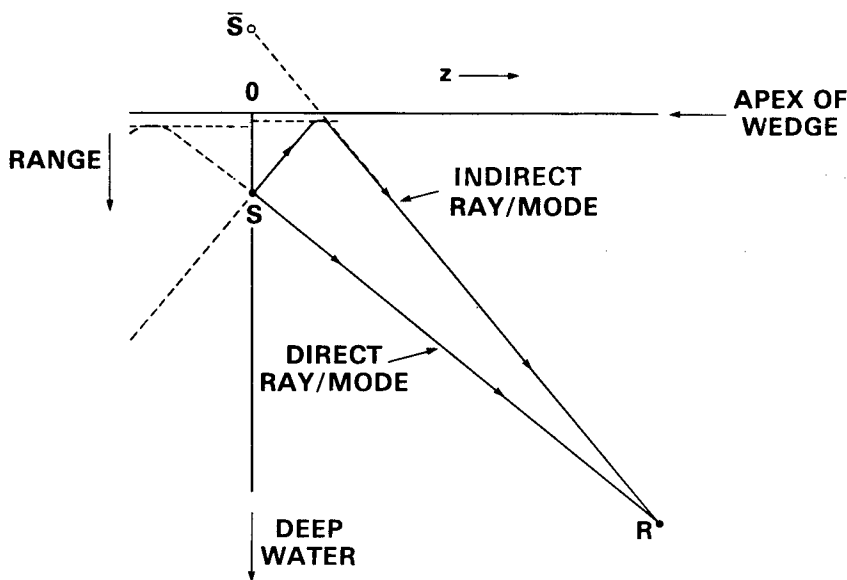


Fig. 11 — Horizontal projection of the direct and indirect ray paths for fixed source and receiver positions

We can now use the definition of a modal ray to interpret the beaming of radiation in the wedge, as predicted by the modal solution. Figure 12 shows upslope propagation with the broken line representing the edge of the beam associated with the first mode. That is, the broken line is the same as the solid hyperbola in Fig. 9 obtained from the modal solution. The solid lines in Fig. 12 represent a few of the first-mode rays, each of which is launched from the source at a different azimuthal angle. Notice that the modal rays fall precisely within the beam. Whichever description of the field is used, either modes or rays, the energy associated with a given mode falls in the same well-defined region, beyond which are shadow zones. This beaming of the radiation can now be understood from the ray argument to be due entirely to ray curvature arising from the repeated acoustic interactions with the inclined surface and bottom planes. The curvature is such that no radiation showing constructive interference characteristic of the  $m$ th mode can extend into the region beyond the beam associated with the  $m$ th mode. Naturally, if a point receiver is placed anywhere within a modal beam, such as at point A in Fig. 12, only two of the modal rays will be incident upon it, as indicated by the double-headed arrows. The beam itself, of course, is comprised of many modal rays.

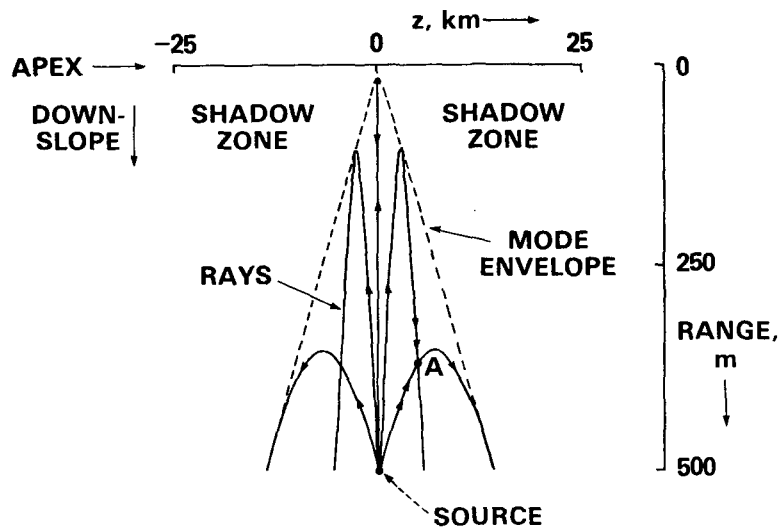


Fig. 12 — Upslope propagation showing the convergent first-mode envelope and some first-mode rays

## EXPERIMENTAL EVIDENCE

The beaming of radiation in the wedge that is predicted theoretically has been observed experimentally. A. B. Wood [11], in one of his model tank experiments, examined the field in a wedge-shaped domain. The tank he used was several feet long with a depth of six or so inches, and the wedge was formed by a sheet of glass inclined at an appropriate angle to the water surface. To record the field upslope of the source, he used a novel technique which is appealing in its simplicity. He first painted the glass sheet with a water soluble paint (distemper), waited until it had dried but not hardened, and then placed the sheet in the tank to form the wedge. He found that the sound field left an impression in the paint.

Figure 13 shows the result of one of A. B. Wood's experiments. The photograph is deliberately inverted in order to have the same orientation as the previous figures, with the apex of the wedge running horizontally along the top and the source located at the bottom. The interference pattern displayed by the field is easily visible in the figure, but the most prominent feature is the convergent beam running towards the apex. It is difficult to make a quantitative comparison between the observed



Fig. 13 — Acoustic field observed by A. B. Wood  
in a wedge-shaped domain [11]\*

beam shape and that predicted theoretically because not enough information is available on the experimental arrangement. The overall features of the measured radiation field are, however, consistent with the theory.

### CONCLUDING REMARKS

The mode and ray descriptions of the acoustic field in a wedge with perfectly reflecting boundaries are complementary. The modal solution gives a complete description of the field, including the phase, and is thus appropriate to calculations of spatial coherence, array performance, and related topics. The dual description, in terms of rays, gives a pictorial view of the field which provides a valuable intuitive understanding of propagation phenomena in the wedge. The formation of shadow zones, for example, has a simple physical interpretation in terms of modal rays.

A new solution for the field in the perfect wedge has been presented here which is valid throughout the ensonified regions. It is possible to derive this solution because the Helmholtz equation for the problem is separable. By way of contrast, the Helmholtz equation for the penetrable wedge is not separable. This implies a degree of complexity beyond that encountered in the perfect wedge problem. Indeed, this is to be expected because when one boundary is penetrable there are critical angle effects with which to contend, and even for those rays which undergo total internal reflection, there is a phase change on reflection from the boundary. Despite these difficulties, it is possible to obtain an

\*Journal of the Acoustic Society of America, 31 (1959), used by permission.

approximate solution for the field in the penetrable wedge by using the perfect solution derived here in conjunction with an argument which relies heavily on the duality between rays and modes. This will be discussed in a future publication.

## ACKNOWLEDGMENTS

I acknowledge with thanks my hosts at NRL for providing a hospitable and stimulating working environment. In particular, I am grateful to Dr. F. Ingenito for many useful discussions on the wedge problem.

## REFERENCES

1. A. Sommerfeld, *Partial Differential Equations in Physics* (Academic Press, New York, 1949) (§17).
2. M.A. Biot and I. Tolstoy, "Formulation of Wave Propagation in Infinite Media by Normal Coordinates with an Application to Diffraction," *J. Acoust. Soc. Am.* **29**, 381-391 (1957).
3. D.L. Bradley and A.A. Hudimac, "The Propagation of Sound in a Wedge Shaped Shallow Duct," Naval Ord. Lab. Rept. NOLTR 70-235, Nov. 1970 (unpublished); D.L. Bradley, Catholic Univ. Am., Washington D.C., 1970.
4. R.D. Graves, A. Nagl, H. Überall, and G.L. Zarur, "Range-Dependent Normal Modes in Underwater Sound Propagation: Application to the Wedge-Shaped Ocean," *J. Acoust. Soc. Am.* **58**, 1171-1177 (1975).
5. A. Papoulis, *Systems and Transforms with Applications in Optics* (McGraw-Hill, 1968), Chapt. 5.
6. N.N. Lebedev, *Special Functions and Their Applications* (Prentice-Hall, 1965), Chapt. 5.
7. G.N. Watson, *A Treatise on the Theory of Bessel Functions*, Second Edition (Cambridge University Press, 1958), p. 416.
8. C.H. Harrison, "Acoustic Shadow Zones in the Horizontal Plane," *J. Acoust. Soc. Am.* **65**, 56-61 (1979).
9. D.E. Weston, "Horizontal Refraction in a Three-Dimensional Medium of Variable Stratification," *Proc. Phys. Soc.* **78**, 46-52 (1961).
10. D.E. Weston, "Guided Propagation in a Slowly Varying Medium," *Proc. Phys. Soc.* **73**, 365-384 (1959).
11. A.B. Wood, "Model Experiments on Sound Propagation in Shallow Seas," *J. Acoust. Soc. Am.* **31**, 1213-1235 (1959).
12. I.S. Gradshteyn and I.M. Ryzhik, *Table of Integrals, Series and Products*, 4th ed. (Academic Press, New York, 1965).
13. P.M. Morse and H. Feshbach, *Methods of Theoretical Physics*, (McGraw-Hill, New York, 1953), p. 631.

**Appendix A**  
**EVALUATION OF THE NORMAL MODE INTEGRAL**

The inversion integral giving the amplitudes of the normal modes (Eq. (19) in the text) is

$$I_\nu = \frac{1}{\pi R_0} \int_0^\pi \frac{\cos \nu \sigma \exp[-jkR_0(1 - 2a \cos \sigma)^{1/2}]}{(1 - 2a \cos \sigma)^{1/2}} d\sigma, \quad (\text{A1})$$

where  $a$  and  $R_0$  are as defined in Eq. (20). Now, with

$$x = \cos \sigma, \quad (\text{A2})$$

we are interested in the function

$$\rho(x) \equiv (1 - 2ax)^{1/2} = (1 - 2ax_0)^{1/2} \left[ 1 + \frac{a(x_0 - x)}{(1 - 2ax_0)} + \dots \right], \quad (\text{A3})$$

where the term on the right is the Taylor expansion of  $\rho(x)$  about  $x = x_0$ . On splitting the range of integration into two, and setting  $x_0 = 1$  in the first interval and  $x_0 = -1$  in the second (these values correspond to the turning points in  $\rho(x)$ ), the integral in Eq. (A1) can be expressed as

$$I_\nu = \frac{1}{\pi R_1} \int_0^{\pi/2} \cos \nu \sigma \exp[-jkR_1[1 + b_1(1 - \cos \sigma) + \dots]] d\sigma \\ + \frac{1}{\pi R_2} \int_{\pi/2}^\pi \cos \nu \sigma \exp[-jkR_2[1 - b_2(1 + \cos \sigma) + \dots]] d\sigma, \quad (\text{A4})$$

where

$$R_1 = R_0(1 - 2a)^{1/2}, \quad R_2 = R_0(1 + 2a)^{1/2} \quad (\text{A5a})$$

$$b_1 = a/(1 - 2a), \quad b_2 = a/(1 + 2a) \quad (\text{A5b})$$

and  $\rho(x)$  in the denominator has been approximated by the first term in the expansion in Eq. (A3). The two components of  $I_\nu$  can now be written in the form

$$I_\nu = \frac{\exp[-jkR_1(1 + b_1)]}{\pi R_1} I_1 + \frac{\exp[-jkR_2(1 - b_2)]}{\pi R_2} I_2, \quad (\text{A6})$$

where

$$I_1 = \int_0^{\pi/2} \cos \nu \sigma \exp[j(kR_1 b_1 \cos \sigma)] d\sigma \quad (\text{A7a})$$

and

$$I_2 = \int_{\pi/2}^\pi \cos \nu \sigma \exp[j(kR_2 b_2 \cos \sigma)] d\sigma. \quad (\text{A7b})$$

In these expressions, the terms beyond those shown in the expansions in Eq. (A4) have been neglected. This is justified because the major contributions to the integrals in Eq. (A4) come from around the turning points of  $\rho(x)$ , where only those terms shown are significant.

With a little algebraic manipulation, the integrals in Eq. (A7) can be expressed as standard forms which can be found in most tables of integrals (e.g., Ref. 12). For  $\nu$  an integer, the results are

$$I_1 = \frac{\pi}{2} \exp\left[j \frac{\nu\pi}{2}\right] H_\nu^{(1)}(kR_1 b_1) \quad (\text{A8a})$$

and

$$I_2 = \frac{\pi}{2} \exp\left[j \frac{\nu\pi}{2}\right] H_\nu^{(2)}(kR_2 b_2), \quad (\text{A8b})$$

which, when substituted into Eq. (A6) give

$$I_\nu = \frac{1}{2} \exp j \frac{\nu\pi}{2} \left[ \frac{\exp [-jkR_1(1+b_1)] H_\nu^{(1)}(kR_1b_1)}{R_1} + \frac{\exp [-jkR_2(1-b_2)] H_\nu^{(2)}(kR_2b_2)}{R_2} \right]. \quad (\text{A9})$$

This is the result in Eq. (21a) in the text that we set out to prove.

## Appendix B THE FIELD IN THE VICINITY OF THE SOURCE

The field from a point source within a bounded domain shows a singularity at the source point, and in the immediate vicinity of this point it has the same form as the free field of the source. Indeed, this fact is often employed to construct solutions for boundary value problems: the field is represented as a superposition of the free-field component and another component chosen to satisfy the boundary conditions.

In the case of the wedge, the solution for the field in Eqs. (15) and (21a) has been derived by using transform methods, rather than the superposition technique, but it should nevertheless be valid in the immediate vicinity of the source point. That is, the modal sum in this region should reduce to the free-field form. We show here that this is the case.

When the receiver is very close to the source, only the term containing the Hankel function of the first kind in Eq. (21a) is significant. This Hankel function has a large argument ( $kR_1b_1$ ) and a large order  $\nu$ . Bearing in mind that at the source point there is a finite number of propagating modes (see Eq. (28) in the text), it is always possible to choose  $kR_1b_1 > \nu$ . ( $kR_1b_1$  increases as the source point is approached). On setting

$$kR_1b_1 = \nu \sec \beta, \quad (\text{B1})$$

the Hankel function of the first kind can be expressed approximately (see Ref. B1) as

$$H_\nu^{(1)}(kR_1b_1) = H_\nu^{(1)}(\nu \sec \beta) = \sqrt{\frac{2}{\pi \nu \tan \beta}} \exp \left\{ j \left[ \nu (\tan \beta - \beta) - \frac{\pi}{4} \right] \right\}. \quad (\text{B2})$$

From the definition of  $\beta$  in Eq. (B1), we have

$$\tan \beta - \beta = -\pi/2 + \frac{kR_1b_1}{\nu} + \frac{\nu}{2kR_1b_1} + \dots \quad (\text{B3})$$

Assuming that  $\nu/(kR_1b_1) \ll 1$  for all  $\nu$ , so that the series may be truncated as shown, this gives

$$H_\nu^{(1)}(kR_1b_1) \approx \sqrt{\frac{2}{\pi kR_1b_1}} \exp \left\{ -j \left[ \frac{\nu\pi}{2} - kR_1b_1 - \frac{\nu^2}{2kR_1b_1} + \frac{\pi}{4} \right] \right\}. \quad (\text{B4})$$

Thus the expression for  $I_\nu$  in Eq. (21a) can be approximated as

$$I_\nu = (2\pi kR_1b_1)^{-1/2} \frac{\exp(-jkR_1)}{R_1} \exp(-j\pi/4) \exp \left( j \frac{\nu^2}{2kR_1b_1} \right). \quad (\text{B5})$$

When this substituted into Eq. (15), the expression for the field becomes

$$\phi = \frac{Q}{\theta_0} (2\pi kR_1b_1)^{-1/2} \frac{\exp(-jkR_1)}{R_1} \exp(-j\pi/4) \sum_\nu \sin \nu \theta \sin \nu \theta' \exp \left( j \frac{\nu^2}{2kR_1b_1} \right). \quad (\text{B6})$$

To evaluate the summation in Eq. (B6), we first employ the trigonometric identity

$$\sin \nu \theta \sin \nu \theta' = 1/2 [\cos \nu(\theta - \theta') - \cos \nu(\theta + \theta')], \quad (\text{B7})$$

but retain only the difference term, since the remaining term makes a negligible contribution to the field when  $\theta \rightarrow \theta'$ . The sum in Eq. (B6) can therefore be written in the form

$$S = \frac{1}{2} \sum_{\nu} \cos \nu(\theta - \theta') \exp\left\{j \frac{\nu^2}{2kR_1 b_1}\right\}. \quad (\text{B8})$$

By expressing the cosine function as the sum of two exponentials, this sum can be written as

$$S = \frac{1}{4} (S_+ + S_-), \quad (\text{B9})$$

where

$$S_{\pm} = \sum_{m=1}^M \exp\left\{j \left[ \pm \frac{m\pi}{\theta_0} (\theta - \theta') + \frac{m^2 \pi^2}{2\theta_0^2 kR_1 b_1} \right]\right\}. \quad (\text{B10})$$

Here we have substituted  $\nu = m\pi/\theta_0$ , and the upper limit on the summation is given by Eq. (28). Now, provided the maximum value of the term containing  $m^2$  in the argument of the exponential function in Eq. (B10) is greater than unity,  $S_{\pm}$  may be approximated by the following integral:

$$S_+ = S_- = \frac{1}{\sqrt{u}} \int_0^{\infty} \exp\left\{j \left[ y^2 + \frac{2wy}{\sqrt{u}} \right]\right\} dy, \quad (\text{B11})$$

where

$$u = \frac{\pi^2}{\theta_0^2 2kR_1 b_1}, \quad 2w = \frac{\pi}{\theta_0} (\theta - \theta'). \quad (\text{B12})$$

The integral in Eq. (B11) is a standard form [B2] which can be expressed exactly in terms of Fresnel integrals. However, in the limit as  $\theta \rightarrow \theta'$  (which is our case) the contribution from the Fresnel integrals falls to zero, and we find that

$$2S = S_+ = S_- = \frac{1}{2} \sqrt{\frac{\pi}{u}} \exp\left[-j \frac{w^2}{u}\right] \exp(j\pi/4). \quad (\text{B13})$$

When this expression for  $S$  is substituted into Eq. (B6), in place of the summation, the field in the vicinity of the source is found to be

$$\phi = \frac{Q}{4\pi} \frac{\exp(-jkR_1)}{R_1} \exp\left[-j \frac{w^2}{u}\right]. \quad (\text{B14})$$

The argument of the second exponential function in this expression is now

$$\begin{aligned} \frac{w^2}{u} &= kR_1 b_1 \frac{(\theta - \theta')^2}{2} = kR_1 b_1 \left[ 1 - \left[ 1 - \frac{(\theta - \theta')^2}{2} \right] \right] \\ &\simeq kR_1 b_1 [1 - \cos(\theta - \theta')], \end{aligned} \quad (\text{B15})$$

where the approximation holds because we are specifically interested in the case where  $\theta \rightarrow \theta'$ . Now, if  $R$  is the distance between the source and the receiver, then

$$\begin{aligned} R^2 &= r^2 + r'^2 + z^2 - 2rr' \cos(\theta - \theta') \\ &= R_1^2 + 2rr'[1 - \cos(\theta - \theta')] \end{aligned} \quad (\text{B16})$$

so that

$$\begin{aligned} \frac{rr'}{R_1} [1 - \cos(\theta - \theta')] &= \frac{R^2 - R_1^2}{2R_1} = \frac{(R - R_1)(R + R_1)}{2R_1} \\ &\simeq (R - R_1) \end{aligned} \quad (\text{B17})$$

where the approximation is valid because in the immediate vicinity of the source  $R = R_1$ . Since  $kR_1 b_1 \equiv krr'/R_1$ , it follows from Eqs. (B15) and (B17) that

$$\frac{w^2}{u} = (R - R_1), \quad (\text{B18})$$

and hence the expression for the field in Eq. (B14) takes the form

$$\phi = \frac{Q}{4\pi} \frac{\exp(-jkR)}{R}, \quad (\text{B19})$$

where the denominator has been written as  $R$  rather than  $R_1$ . But the expression in Eq. (B19) is precisely the free-field produced by the source, which is what we set out to prove. Note that Bradley and Hudimac's [B3] solution for the field in the wedge (Eq. (23)) does not reduce to the required form in the vicinity of the source point.

#### REFERENCES

- B1. P.M. Morse and H. Feshbach, *Methods of Theoretical Physics*, (McGraw-Hill, New York, 1953), p. 631.
- B2. I.S. Gradshteyn and I.M. Ryzhik, *Table of Integrals, Series and Products*, 4th ed. (Academic Press, New York, 1965).
- B3. D.L. Bradley and A.A. Hudimac, "The Propagation of Sound in a Wedge Shaped Shallow Duct," Naval Ord. Lab. Rept. NOLTR 70-235, Nov. 1970 (unpublished); D.L. Bradley, Catholic Univ. Am., Washington D.C., 1970.

### Appendix C MODE/RAY HYPERBOLAE

The two hyperbolic ray paths associated with a particular mode are illustrated in Fig. C1. The parameters of the two curves are derived below.

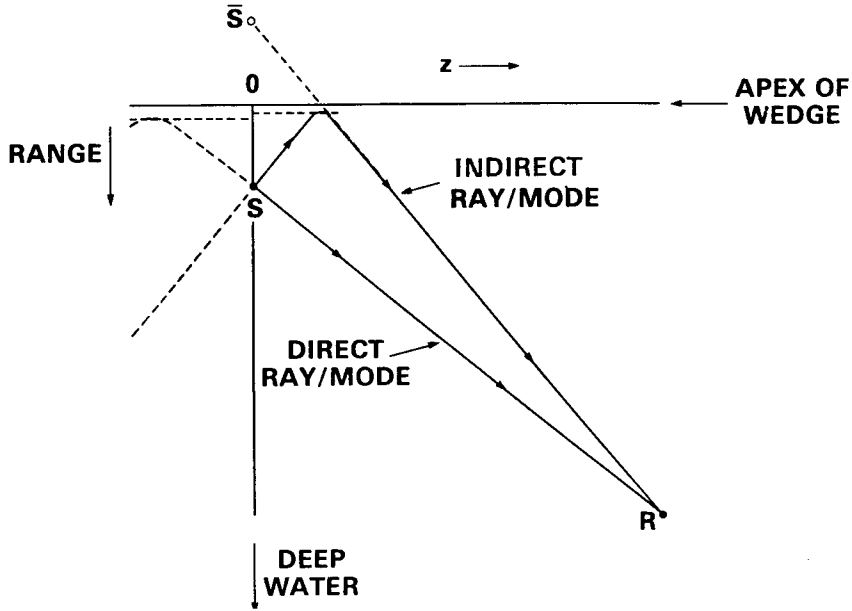


Fig. C1 — Horizontal projection of the direct and indirect ray paths for fixed source and receiver positions

Let the point  $(\bar{r}, \bar{z})$  fall on one of the hyperbolae. The Eq. for the hyperbola can then be written as

$$\frac{\bar{r}^2}{r_m^2} - \frac{(\bar{z} - z_m)^2}{b_m^2} = 1, \quad (C1)$$

where  $r_m$ ,  $b_m$ , and  $z_m$  are the parameters of the hyperbolae associated with the  $m$ th mode. These parameters take dual values, corresponding to the two ray paths.

From shallow water theory, the grazing angle  $\alpha_m$  of the  $m$ th mode at the turning point is given by

$$\sin \alpha_m = \frac{m\pi}{kr_m\theta_0} = \frac{q_m}{r_m}, \quad (C2)$$

where  $r_m\theta_0$  is just the depth at the vertex of the hyperbola, and  $q_m = m\pi/(k\theta_0)$ . Now, the angle between the apex of the wedge and the asymptotes of the hyperbola is also equal to  $\alpha_m$  [C1], and hence we have

$$\tan \alpha_m = \frac{r_m}{b_m}. \quad (C3)$$

It follows from Eqs. (C2) and (C3) that

$$b_m = \frac{r_m}{q_m} (r_m^2 - q_m^2)^{1/2}. \quad (C4)$$

We now require two more conditions to determine the three parameters of the hyperbola. They are that the curve must pass through the source point  $(r', 0)$  and the receiver point  $(r, z)$  (both rotated onto the surface). These conditions lead to the equations

$$\frac{r'^2}{r_m^2} - \frac{z_m^2}{b_m^2} = 1 \quad (C5)$$

and

$$\frac{r^2}{r_m^2} - \frac{(z - z_m)^2}{b_m^2} = 1. \quad (C6)$$

On eliminating  $z_m$  from these equations, we find that

$$z = [(r^2 - r_m^2)^{1/2} \pm (r'^2 - r_m^2)^{1/2}](r_m^2 - q_m^2)^{1/2}/q_m. \quad (C7)$$

Assuming that  $r^2 \gg r_m^2$ ,  $r'^2 \gg r_m^2$  and  $r \neq r'$ , then Eq. (C7) may be easily solved to give

$$r_m = q_m \left[ 1 + \frac{z^2}{(r \pm r')^2} \right]^{1/2}. \quad (C8)$$

Simple algebra shows that the remaining two parameters are given by the expressions

$$z_m = \pm \left\{ r'^2 - q_m^2 \left[ 1 + \frac{z^2}{(r \pm r')^2} \right] \right\}^{1/2} \frac{z}{(r \pm r')} \quad (C9)$$

and

$$b_m = \left[ 1 + \frac{z^2}{(r \pm r')^2} \right]^{1/2} \frac{q_m^2}{(r \pm r')}. \quad (C10)$$

Where there is a choice of sign in Eqs. (C8) to (C10), which are the results we require, the plus sign relates to the indirect ray path and the minus sign to the direct ray path.

## REFERENCES

- C1. D.E. Weston, "Horizontal Refraction in a Three-Dimensional Medium of Variable Stratification," Proc. Phys. Soc. **78**, 46-52 (1961).

